An advanced Photovoltaic Thermal Collector Storage Solar Water Heating based on planar liquid vapour thermal diode: Model-based design approach for the optimal energy performance assessment

Energy Reports 10 (2023) 4616–4628

Contents lists available at ScienceDirect

Energy Reports

journal homepage: www.elsevier.com/locate/egyr

An advanced Photovoltaic Thermal Collector Storage Solar Water Heating based on planar liquid vapour thermal diode: Model-based design approach for the optimal energy performance assessment

Annamaria Buonomanoa [a], Cesare forzano [a,*], Adrian Pugsley [b], Mervyn Smyth [b]

[a] Department of Industrial Engineering, University of Naples Federico II, Naples, Italy
[b] School of Architecture and the Built Environment, Ulster University, Belfast, UK

ARTICLE INFO

Keywords:
Thermal diode
One-way heat transfer
ICSSWHs
Heat collection
Heat retention
Dynamic simulation

ABSTRACT

The building sector is responsible for the highest portion of energy consumption and carbon dioxide emissions. To partly address this issue, the scientific community is placing greater emphasis on the utilization of Building Integrated Solar Systems (BISS) as a means of improving building thermophysics and decreasing primary energy demand. Within this framework, Integrated Collector Storage Solar Water Heaters (ICSSWH) have the potential to significantly decrease the costs associated with the installation and maintenance of building-integrated solar systems (BISS), all while optimizing the utilization of solar power. Nevertheless, ICSSWHs exhibit certain limitations in their capacity to retain thermal energy, particularly during nocturnal periods. One potential approach for enhancing the efficiency of ICSSWH collectors involves the integration of Thermal Diodes (TD), which have the capability to optimize heat absorption while minimizing heat retention. In this context, to advance the state-of-the-art in the field, this paper presents a novel dynamic simulation tool conceived to assess the performance of an innovative Hybrid Photovoltaic Thermal ICSSWH (the HyPVT), incorporating a cutting-edge Planar Liquid Vapour Thermal Diode (PLVTD), and purposely designed to be integrated into buildings' envelope. By using the developed simulation tool, the performance of the proposed HyPVT collector concept is investigated with the aim of assessing its collection and retention efficiencies under different boundary and operating conditions. Furthermore, to show the effect of the Planar Liquid Vapour Thermal Diode (PLVTD) adoption, a comparative analysis is conducted between the proposed ICSSWH and a conventional one (without a thermal diode). Finally, the developed tool will be utilized in forthcoming research to determine the optimal device configuration through the utilization of a model-based design methodology.

1. Introduction

Reducing energy consumption and related CO_2 emissions are the main challenges of this time. In this setting, great effort is being made by many researchers to boost the sustainability of a wide range of sectors, such as buildings (Forzano et al., 2019; Vassiliades et al., 2022), sustainable communities (Barone et al., 2021b; Maturo et al., 2021; Ceglia et al., 2022; Bakhtavar et al., 2020; Barone et al., 2021; Buonomano et al., 2023a) and transport systems (Barone et al., 2021a, 2020; Martínez Fernández et al., 2019; Zhang et al., 2019; Buonomano et al., 2002). Specifically, buildings are responsible for up to 40% of the total primary energy consumption and CO_2 emissions worldwide (Agency, 2003; International Energy Agency, I.E.A., 2014), representing the highest relative share. Consequently, more and more challenging emission reduction targets and renewable energy goals for the building sector have been set by European institutions, such as the Directive (EU) 2018/2001 (Graziani, 2017). In this framework, solar-based renewable technologies have considerable potential in aiding the sector to reach this goal (Barone et al., 2019; Buonomano et al., 2023b), especially considering the case of Building Integrated Solar Thermal Systems (BISTS) (Lamnatou et al., 2018; Gagliano et al., 2021). Indeed, BISTS have been proven to be a promising solution for residential and commercial buildings, for both space heating (and cooling) and domestic hot water production, as indicated by the number of works present in the scientific literature (Baljit et al., 2016; Chandrasekar and Senthilkumar, 2021; Ghosh, 2020). Among the feasible technologies that can be

* Correspondence to: University of Naples Federico II, Department of Industrial Engineering, P.le Tecchio 80, 80125 Naples, Italy.
E-mail address: cesare.forzano@unina.it (C. forzano).

https://doi.org/10.1016/j.egyr.2023.09.078
Received 6 April 2023; Received in revised form 30 August 2023; Accepted 13 September 2023
Available online 18 November 2023

integrated into the building envelope, Integrated Collector-Storage Solar Water Heaters (ICSSWH), which are characterized by reduced system size and cost (Tripanagnostopoulos and Souliotis, 2006), due to the coupling in one chasing of the collector surface and of the heat transfer fluid storage tank, represent a very promising solution.

Integrated Collectors Storage Solar Water Heaters

ICSSWHs are commonly adopted in hot climatic zones, and have been increasingly studied by the scientific community with the ultimate aim of improving their efficiency, as demonstrated by the number of related review and research papers (Sharma and Chauhan, 2022; Anupam Rao and Somwanshi, 2022; Singh et al., 2016). One specific example is given in Xie et al. (2022) where the authors present a hybrid photovoltaic/thermal ICSSWH, characterized by a compact structure and a low initial cost, using an insulated water tank directly coupled with a PV panel. The device was subjected to various tests, that concluded that the device performance was significantly linked to the ambient air temperature. A thermal only ICSSWH, characterized by an evacuated gap between the glass cover and the absorber, was investigated by the authors of Barone et al. (2022) using simulations. From the conducted analysis, it was possible to conclude that interesting energy and emissions savings are achievable by adopting the proposed device. Vacuum technology is also exploited and investigated in a study involving a cylindrical ICSSWH (Messaouda et al., 2020) equipped with a concentrator. The device consisted of two concentric cylinders, one acting as an absorber/storage tank and the other as encasing glass cover and both separated by an evacuated gap. The experimental and simulation study concluded that significant heat retention performance can be achieved by exploiting the vacuum. Another device using a compound parabolic solar concentrator (no vacuum) and Integrated Collector Storage solar water heater was experimentally evaluated in Panahi et al. (2019). The authors state that the concentrator substantially improves the collection efficiency during the day, but the nighttime heat storage retention is strongly influenced by the temperature gradient between the ambient air and water. A planar integrated solar water heater with corrugated absorber was experimentally investigated in Yassen et al. (2019). Similar to other works, the authors state that worthy efficiencies are obtained during the collection period, but that large thermal losses were experienced during the night. Many other studies exist in the literature, irrespective of the geometry and/or technology, agreeing with the general view that during the day (namely forward or collection mode) ICSSWHs exhibit positive collection efficiencies, but conversely, during non-collection periods (namely reverse or retention mode) they are not capable of storing the heat efficiently, and thus they are a viable proposition in hot climate regions and applications with no prolonged thermal storage. This behaviour is strictly linked to the fact that, even if lower fabrication, installation, and maintenance costs are achievable, ICSSWH/tanks collectors installed externally are exposed to external weather that produce high heat losses. To overcome such issues, it is necessary to develop methods that promotes heat transfer in one direction during the collection phase and limits heat losses during the retention one. A possible solution explored by the scientific community is the integration of thermal diodes into the ICSSWH configuration.

ICSSWH incorporating thermal diode technology The word "thermal diode" refers to a technology capable of promoting heat transfer in one direction whilst reducing/stopping it in the other. This characteristic perfectly matches the need of ICSSWHs requiring a way to boost heat collection whilst minimizing heat losses during the retention phase. Diverse are the works in literature discussing the possibility of using thermal diode technology in ICSSWH (Anupam Rao and Somwanshi, 2022; Singh et al., 2016). Initial work based on a triangular ICSSWH integrating thermal diode is presented in Mohamad (1997). The authors conclude, after experimental analysis, that the proposed device has a collection performance comparable to similar collectors (without the thermal diode) but produces higher performance in terms of heat retention during the night. The convenience in using a thermal diode was investigated in Sopian et al. (2004) for a non-metallic unglazed solar water heater ICS system. Specifically, an experimental comparison between the ICS collector with and without the thermal diode demonstrated that the temperature drop during the retention hours was 10 °C less in the thermal diode unit versus the standard ICS collector unit. Another experimental investigation of the heat retention performance of an ICSSWH device is instead reported in Muhumuza et al. (2019b). Here, the device was designed with cylindrical geometry and an integral thermal diode to supply solar hot water to off-grid users. The unit employed an asymmetric reflector with the ICS cylinder in its focus. Analysis indicated a heat retention efficiency of 35% was achievable. Another ICS designed to maximize heat retention performance and also using an asymmetric concentrating reflector is presented in Souliotis et al. (2011, 2017) through a study of a device made from two concentric vessels with the adjoining gap evacuated and enclosing a small volume of heat transfer fluid. From testing, a good performance during the forward phase was measured, and a slightly lower performance during the reverse phase. The cylindrical geometry is also investigated in other studies (Smyth et al., 2020a; Muhumuza et al., 2019a) where a range of hermetically sealed horizontal, cylindrical double vessel ICSSWH prototypes are experimentally evaluated. The results show positive heat collection and retention performances, but also indicate room for further development. A simulation approach was instead adopted in work (Smyth et al., 2020b) using a dynamic simulation tool where a cylindrical ICSSWH with thermal diode is modelled and validated against experimental data. The tool was developed to conduct a comparison between different devices with and without thermal diode technologies. The result of the simulations returned a higher performance for the cylindrical ICSSWH and thermal diode over similar units without the thermal diode. A different device, still using cylindrical geometry was investigated in Smyth et al. (2017, 2018) to determine the collection and retention efficiencies, as well as heat fluxes, using experimental tests performed at an indoor test facility. The results gave collection efficiencies ranging from 33.2% to 41%, depending on the considered time intervals. The authors state that the thermal losses of the prototype were 50% lower than those of similar systems.

Aims and innovation of the current work

From the investigated literature, the interest by the scientific community in ICSSWHs and the integration of Thermal Diodes has been observed (Anupam Rao and Somwanshi, 2022; Singh et al., 2016). Indeed, most works stresses the high performance achievable by such systems, as well as the potential benefits in their application. Nonetheless, two main lacks of knowledge around this topic still exist. The first is that thermal diode ICSSWH research is still in its infancy and thus the topic requires much more investigation to enhance the current state-of-the-art. The second is that the vast majority of the research conducted to date use primarily experimental approach, whereas the use of dynamic simulation is limited (with some exceptions Smyth et al., 2020b). This represents a severe limitation to the progress of this scientific topic. Indeed, compared to experimental approach, having a tool capable of evaluating the device performance under diverse boundary and operating conditions, by also varying its geometrical features, would allow more rapid analysis with a faster identification of the optimal ICSSWH design. In this framework, the present manuscript has two different aims: (i) to develop and experimentally validate a dynamic simulation tool for a novel Planar Liquid Vapour Thermal Diode (PLVTD) prototype, conceived to be included into an ICSSWH. The developed tool can assess the PLVTD behaviour under diverse boundary and working conditions and optimizing the prototype geometry with the aim of boosting its overall performance; (ii) to verify the potential benefits achievable by the integration of the investigated PLVTD into ICSSWH collectors. To do so, a novel dynamic simulation tool for the energy performance investigation of an innovative Hybrid PhotoVoltaic/Thermal ICSSWH collector (named the HyPVT) and integrating the investigated PLVTD, is developed. The resulting dynamic simulation tool can be adopted to simulate the device performance under different boundary conditions

and compare them with a standard ICSSWH with similar geometry, verifying the convenience of the PLVTD adoption. Moreover, the tool can be exploited to perform suitable optimizations which will be used to inform the prototype design and fabrication process. As a future perspective, the prototype, that will be fabricated with the aid of the developed dynamic simulation tool, will be subjected to suitably experimental analyses, the results of which will be exploited to finalize the dynamic simulation tool validation.

2. Planar liquid vapour thermal diode

As previously stated, the word "thermal diode" refers to a technology capable of promoting heat transfer in one direction whilst reducing/stopping it in reverse by varying its thermal resistance (R) depending on the boundary/working conditions. Such a feature is extremely useful in a wide range of applications and has specific potential in ICSSWH (Integrating Collector Solar Storage Water Heaters) devices. This current study presents a novel Planar Liquid Vapour Thermal Diode (PLVTD) designed and experimentally tested at the Centre of Sustainable Technologies, Ulster University (Belfast, Northern Ireland). The developed device will be initially described in terms of its geometrical features and working principles, then, a mathematical model, suitably developed to evaluate the PLVTD performance under different boundary and operating conditions, will be presented together with its experimental validation.

2.1. PLVTD description

The PLVTD concept, structure and components are schematically and visually shown in Fig. 1 and Fig. 2. Specifically, the PLVTD is a hermetically sealed and evacuated stainless-steel vessel (650 × 530 × 100 mm — Fig. 2a) containing a Heat Transfer Fluid – HTF - (water) that exists in liquid and vapour phases in a thermodynamic state close to saturation. To avoid the device collapse due to the vacuum, a stainless-steel pillar structure is created inside it (400 pillars, 8 mm diameter — Fig. 2c). The device is covered with a transparent cover (4 mm thick). Finally, the device's inner surface (the transparent cover on the left of Fig. 1) is coated with a wicking material (a novel fibreglass/carbon fibre fabric in a ratio of 1 to 8 — Fig. 2b) which due to capillary action, ensures that the surface is always wetted by the HTF. Conversely, no wicking material exists on the device other surfaces. It is worth noting that from hereon, the front of the device (the transparent cover) is termed the "evaporator" and the back of the device (bottom of the vessel) is termed the "condenser".

The described PLVTD working principles are schematically represented in Fig. 3 as a function of the device operating conditions. Specifically, it is possible to distinguish between the two different operational modes: (i) forward mode (Fig. 3a) — when the heat is transferred from the evaporator to the condenser ($T_{evaporator} > T_{condenser}$); and (ii) reverse mode (Fig. 3b) — when the heat is transferred from the condenser to the evaporator ($T_{condenser} > T_{evaporator}$). During the forward mode (Fig. 3a) the HTF fluid wetting the hottest plate (evaporator) evaporates, absorbing heat from the surface (thus cooling it down). The generated vapour migrates to the colder plate (condenser) where it condenses, releasing latent heat (heating it). Once the water has condensed, it falls to the lower portion of the vessel where it is re-absorbed by the wicking material, enabling the cycle continuation. During the forward mode, there are three heat transfer mechanisms occurring in parallel: (i) convection, i.e. via evaporation and condensation; (ii) radiation; (iii) conduction through the pillar structure. Reverse mode (Fig. 3b) occurs when the condenser temperature is higher than the evaporator temperature. In this case, the evaporation/condensation phenomena cannot happen since the condenser surface is not wet. In this case, only two heat transfer mechanisms occur in parallel: (i) radiation; and (ii) conduction through the pillar structure.

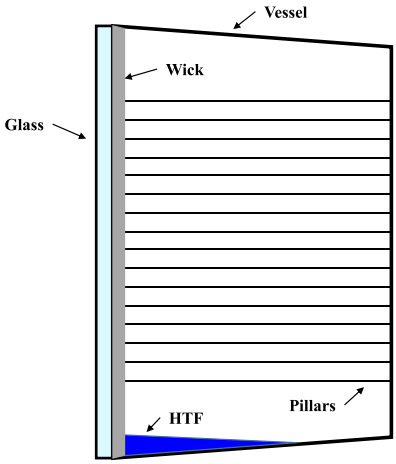

Fig. 1. Thermal diode schematic diagram.

From the described working principle, it is clear that keeping the evaporator wet and the condenser dry is essential to achieving a high thermal transmittance (low thermal resistance) in the forward mode (due to the evaporation and condensation phenomena) and a low thermal transmittance (high thermal resistance) in reverse. In this way, the vacuum guarantees that evaporation and condensation can take place even at temperatures slightly higher than ambient one. This ensures an efficient collection of heat from the absorber surface, with the presence of the wick that generates capillary pressure to transport the fluid from the bottom of the vessel to the top, allowing evaporation to take place continually. An image of the assembled PLVTD prototype is shown in Fig. 4, where the stainless-steel vessel, wicking material/texture and the transparent cover (evaporator surface) are detailed.

2.2. Experimental investigation

To analyse the developed PLVTD behaviour, the unit underwent several experimental tests at the Centre for Sustainable Technologies (CST), Ulster University (Belfast, Northern Ireland). An image of the adopted experimental set-up is shown in Fig. 5a whilst a simplified schematic (showing the thermocouples arrangement) is presented in Fig. 5b. Specifically, in Fig. 5b it is possible to notice the experimental arrangement consisting of the PLVTD placed between two water tanks (front and back) each acting as alternating hot and/or cold sources to recreate the forward and the reverse operating conditions. The two tank temperatures are thermally controlled through two different closed-circuit heating and chilled water systems (two Julaboo1000f units). Furthermore, the spaces between the diode element and the tanks are filled with conductive gel to optimize the thermal contact between the PLVTD and the front and back tanks. Finally, the whole system is then enclosed into several insulation layers made of extruded polystyrene (Fig. 5a) in order to avoid dispersions towards the ambient and improve accuracy of the results.

Within the experimental apparatus there are twenty-four thermocouples (T-type Copper/Constantan) with an accuracy of +/−0.5 °C, which are appliable for the test temperature range (0–300 °C). With respect to the condenser and evaporator surfaces, five thermocouples were placed on the condenser, and thirteen thermocouples were placed on the evaporator. It worth noting that no thermocouples are installed inside the PLVTD due to the difficulties associated with maintaining a perfectly evacuated chamber. A number of different tests were performed to study both forward and reverse operating conditions. In the forward mode tests the front tank (evaporator side) is brought to a higher temperature than the back tank (condenser side). Conversely, to test the reverse mode, the front tank (evaporator side) is brought to a

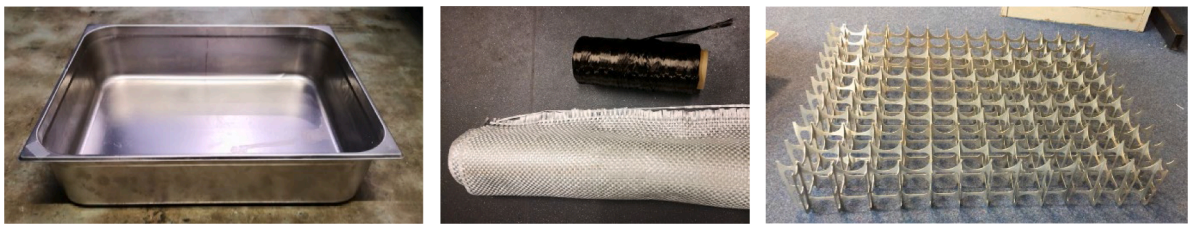

Fig. 2. PLV thermal diode components.

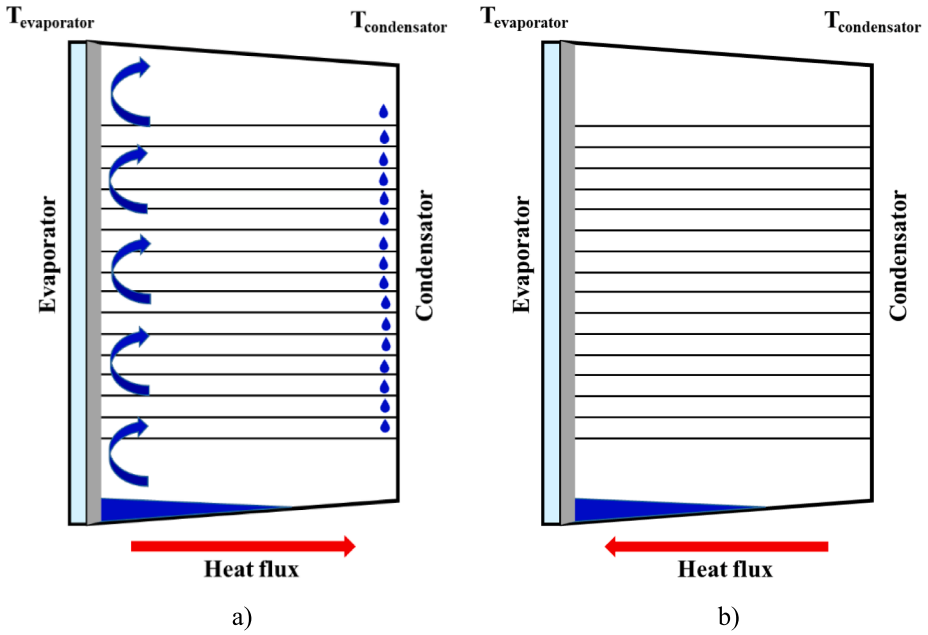

Fig. 3. Thermal diode schematic diagram and operating principles.

Fig. 4. PLV thermal diode prototype.

lower temperature than the back tank (condenser side). The list of conducted tests is shown in Table 1. For the sake of brevity, the results for only a forward and reverse test (Test 1 and Test 4) are reported and shown in Fig. 6a and Fig. 6b, respectively. Here, it is possible to appreciate the thermal history of both evaporator (T_{ev} — blue line) and condenser (T_{con} — orange line) temperature.

2.3. PLVTD mathematical model

To simulate the PLVTD prototype performance under diverse boundary and operating conditions, a mathematical model of the device has been developed and implemented in MatLab environment. The simulation tool, that will be described in this section, relies on three simplified assumptions: (i) negligible heat losses are considered through the lateral insulated surfaces; (ii) the water vapour included in the diode cavity is studied by using the ideal gas model, and (iii) the surfaces are considered as isothermal. Since different behaviours occur in the forward and the reverse operating conditions, two separate thermal networks were considered to study the heat transfer phenomena, as shown in Fig. 7. During the forward mode, the heat transfers from the front of the device (T_1 — external evaporator surface) to the back (T_5 — external condenser surface) as shown in the thermal network Fig. 7a. During the reverse mode, the heat transfers in the opposite direction (from T_5 to T_1) following the thermal network shown in Fig. 7b.

From the figure, it is possible to distinguish different thermal nodes and resistances. Concerning the thermal nodes: T_1 is the external evaporator surface (glass cover); T_2 is the temperature at the interface between the internal evaporator surface and the wick layer; T_3 is the wick layer internal surface; T_4 is the internal evaporator (vessel) surface; and T_5 is the external evaporator (vessel) surface. The thermal resistances, R_{1-2}, R_{2-3}, and R_{4-5} are the conductive thermal resistances through the evaporator, the wicking material and the condenser, respectively. These resistances are evaluated using the following well-known equations:

$$R_{1-2} = \frac{s_{evap}}{k_{evap} A_{diode}} \tag{1}$$

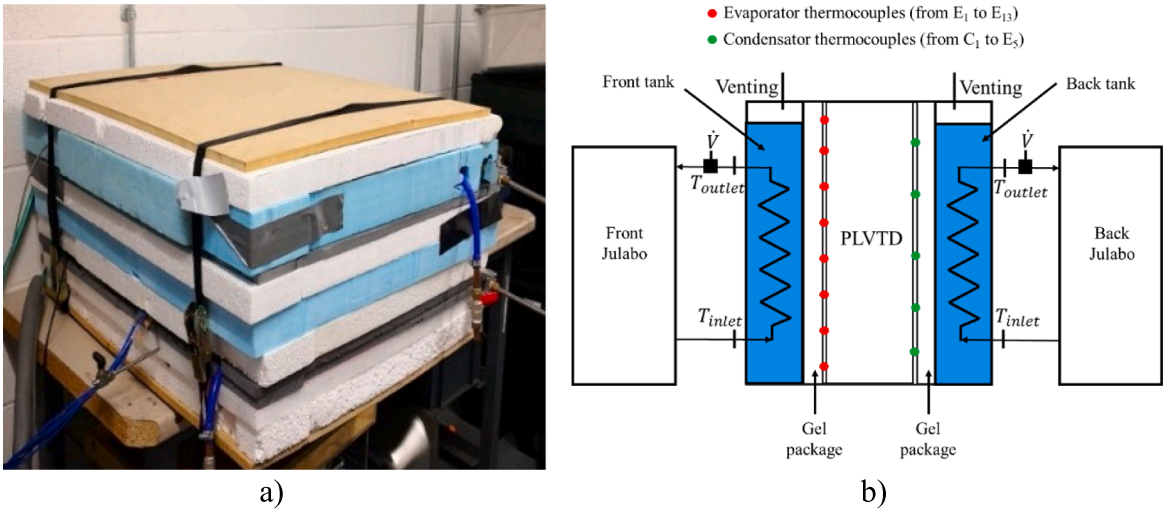

Fig. 5. PLVTD experimental set-up (a) and thermocouple arrangement (b).

Table 1
Conducted experimental tests.

Test number	Test type	Evaporator initial temperature	Condenser initial temperature
		[°C]	
Test 1	Forward	53	36
Test 2	Forward	36	26
Test 3	Reverse	16	45
Test 4	Reverse	15	70

$$R_{2-3} = \frac{s_{wick}}{k_{wick} A_{diode}} \quad (2)$$

$$R_{4-5} = \frac{s_{cond}}{k_{cond} A_{diode}} \quad (3)$$

Where, s_{evap}, s_{wick}, and s_{cond} are evaporator, wick, and condenser thickness, respectively, and k_{evap}, k_{wick}, and k_{cond} are evaporator, wick, and condenser thermal conductivity, respectively. The last resistance, R_{3-4} (not shown in Fig. 7), is the thermal diode equivalent resistance, which is considered different in the forward and reverse modes. During the forward mode, R_{3-4} is the equivalent resistance resulting from three mechanisms occurring in parallel: (i) convection, i.e. via evaporation and condensation phenomena (computed by considering the respective

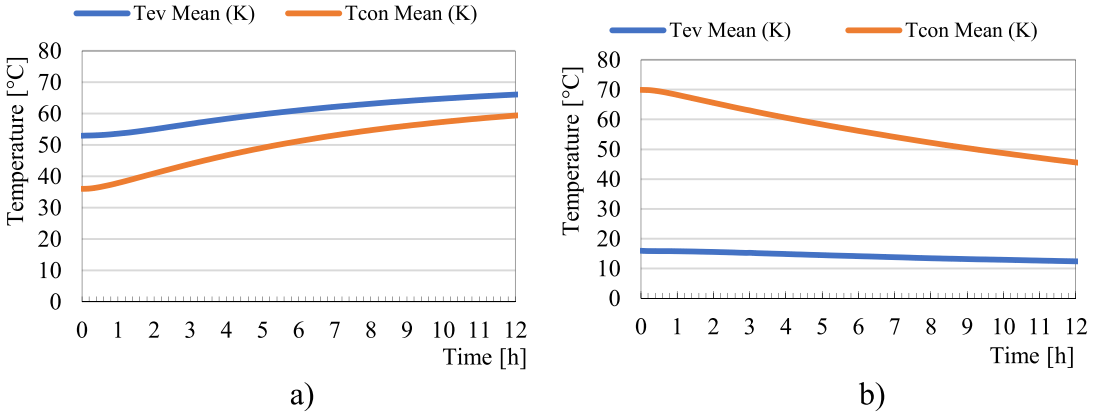

Fig. 6. Test 1 (left) and Test 4 (right) temperature time profiles. (For interpretation of the references to colour in this figure legend, the reader is referred to the web version of this article.)

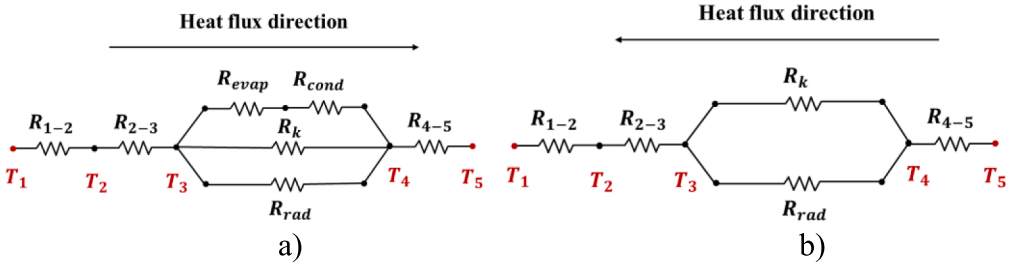

Fig. 7. PLVTD thermal networks: forward mode (a); reverse mode (b).

evaporation and condensation resistances R_{evap} and R_{cond}), (ii) radiation R_{rad}, and (iii) conduction through the pillars R_k. The radiative and conductive resistances through the diode cavity are evaluated as follows:

$$R_{k,diode} = \frac{s_{pillars}}{k_{pillars} A_{pillars}} \tag{4}$$

$$R_{rad,diode} = \frac{\frac{1}{\varepsilon_{evap}} + \frac{1}{\varepsilon_{cond}} + 1}{\sigma A_{TD} \left(T_3^2 + T_4^2\right)(T_3 + T_4)} \tag{5}$$

Where $s_{pillars}$, $k_{pillars}$, and $A_{pillars}$, are the thickness, thermal conductivity, and total area of the pillars respectively, ε_{evap} and ε_{cond} are the emittances of evaporator and condenser, respectively, σ is the Stefan–Boltzman constant, and A_{TD} is the total area of the thermal diode (less the pillars area). Finally, with respect to the evaporation and condensation resistances (R_{evap} and R_{cond} respectively), these are evaluated through the following equations:

$$R_{evap} = \frac{R_{vap} \cdot T_3^2 \cdot \sqrt{2 \cdot \pi \cdot R_{vap} \cdot T_3}}{A_{TD} \cdot Q_L^2(T_3) \cdot P(T_3)} \tag{6}$$

$$R_{cond} = \frac{R_{vap} \cdot T_4^2 \cdot \sqrt{2 \cdot \pi \cdot R_{vap} \cdot T_4}}{A_{TD} \cdot Q_L^2(T_4) \cdot P(T_4)} \tag{7}$$

Where R_{vap} represents the gas constant for water vapour, T_3 and T_4 are the wick and condenser temperatures, respectively, and Q_L and P are the latent heat of evaporation/condensation and the vapour pressure of the water, respectively (both assessed at the corresponding surface temperature). It worth noting that the evaporation and condensation phenomena cannot occur during the reverse mode, since the heat is transferred from the condenser (T_4) to the absorber (T_3), and the condenser is not wet (no wick). Thus, R_{evap} and R_{cond} cannot be considered and so the thermal diode equivalent resistance in forward and reverse mode is evaluated as follows:

$$R_{Eq,diode,Forward} = R_{3-4} = \frac{1}{\left(\frac{1}{R_k} + \frac{1}{R_{rad}} + \frac{1}{\left(R_{evap} + R_{cond}\right)}\right)} \tag{8}$$

$$R_{Eq,diode,Reverse} = R_{3-4} = \frac{1}{\left(\frac{1}{R_k} + \frac{1}{R_{rad}}\right)} \tag{9}$$

Focusing on dynamically assessing the PLVTD behaviour, the described heat transfer equations have been implemented in a MatLab routine. To verify the reliability of the resulting simulation tool, it has been experimentally validated as described in the following paragraph.

2.4. PLVTD model validation

To verify the reliability of the developed PLVTD dynamic simulation tool, an experimental validation was carried out. Simulation data have been compared with those measured from the previously described experimental testing for both forward and reverse operating conditions. In particular, two main temperatures have been taken into account: (i) external surface of the evaporator (T_1 — Fig. 7) and (ii) external surface of the condenser (T_5 — Fig. 7). Note that the other temperatures (those related to the wicking material — T_2 and T_3 in Fig. 7), and the internal surface of the condenser (T_4 in Fig. 7) cannot be considered in the validation due to the difficulty in measuring the related experimental data (thermocouples were no installed in the evacuated chamber due to the risk of vacuum leakage). Nevertheless, by validating the condenser temperature for the forward mode, and absorber temperature for the reverse mode, it is possible to ensure the correct assessment of the thermal diode behaviour. In this context, four experimental tests, previously described in Table 1 have been considered. To validate the device during the forward mode, the evaporator temperature (T_1) is considered as an input of the software, whereas the condenser temperature output (T_5) is subjected to the validation. The opposite action occurs in validating the device during the reverse mode. The comparison between the experimental and simulated data time histories are shown in Fig. 8, Fig. 9, Fig. 10, and Fig. 11.

For the forward tests (Fig. 8 and Fig. 9), the experimental condenser temperature (dotted black lines) and the simulated temperature (solid red lines) exhibit a very good agreement, with the deviation always below 1 °C (dotted purple lines). Similarly, for the reverse tests (Fig. 10 and Fig. 11), the experimental evaporator temperature (dotted black lines) and the simulated temperature (solid red lines) also present a very good agreement with the temperature deviations (dotted purple lines) almost always below 1 °C. To further prove the reliability of the developed simulation tool, a statistical analysis has been conducted to assess the goodness of fit between experimental and simulated data. In particular, the two indexes considered are the mean absolute percentage error (MAPE), and the R-squared (R^2), evaluated as follows:

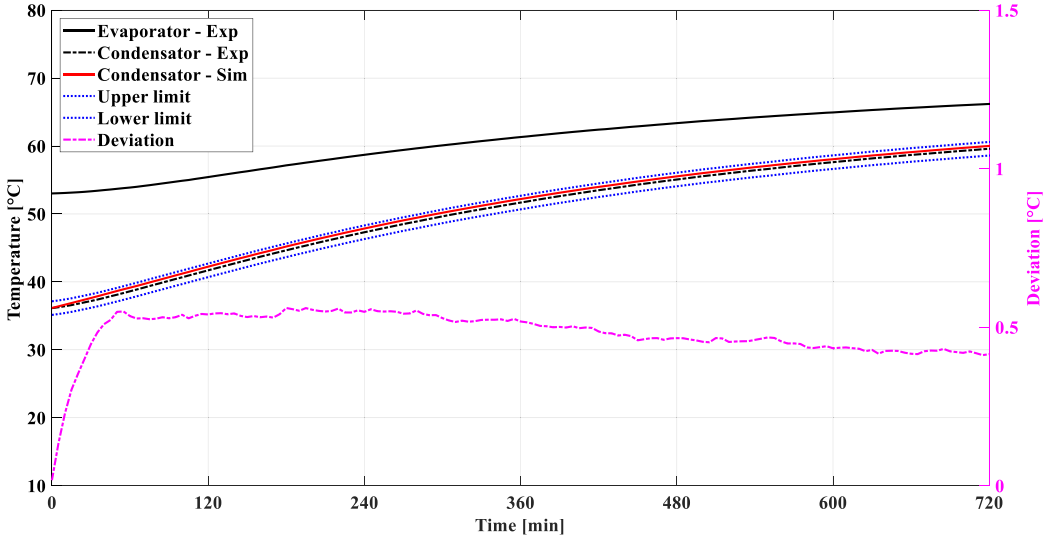

Fig. 8. Test 1 (forward), experimental vs. Simulated temperature time histories. (For interpretation of the references to colour in this figure legend, the reader is referred to the web version of this article.)

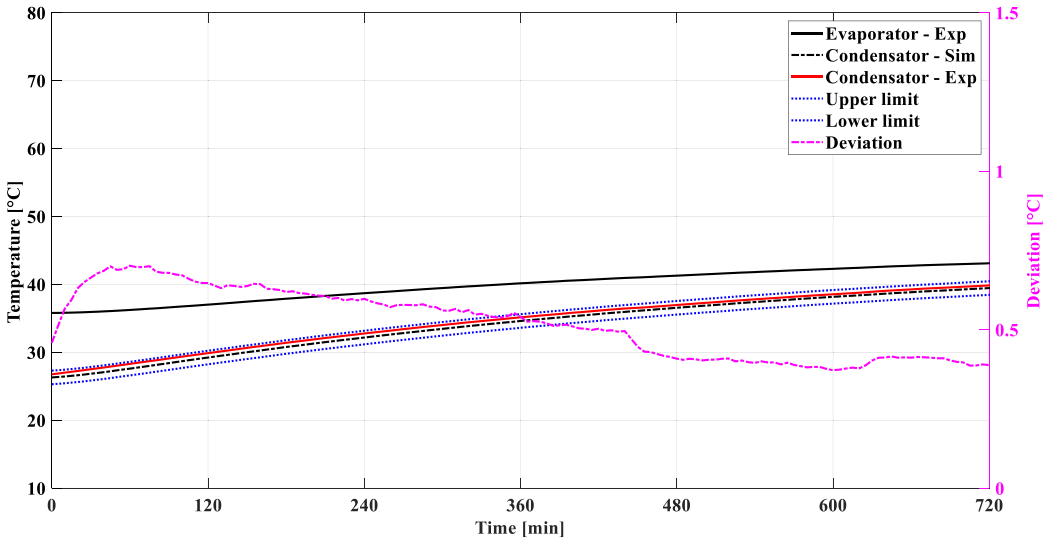

Fig. 9. Test 2 (forward), experimental vs. Simulated temperature time histories. (For interpretation of the references to colour in this figure legend, the reader is referred to the web version of this article.)

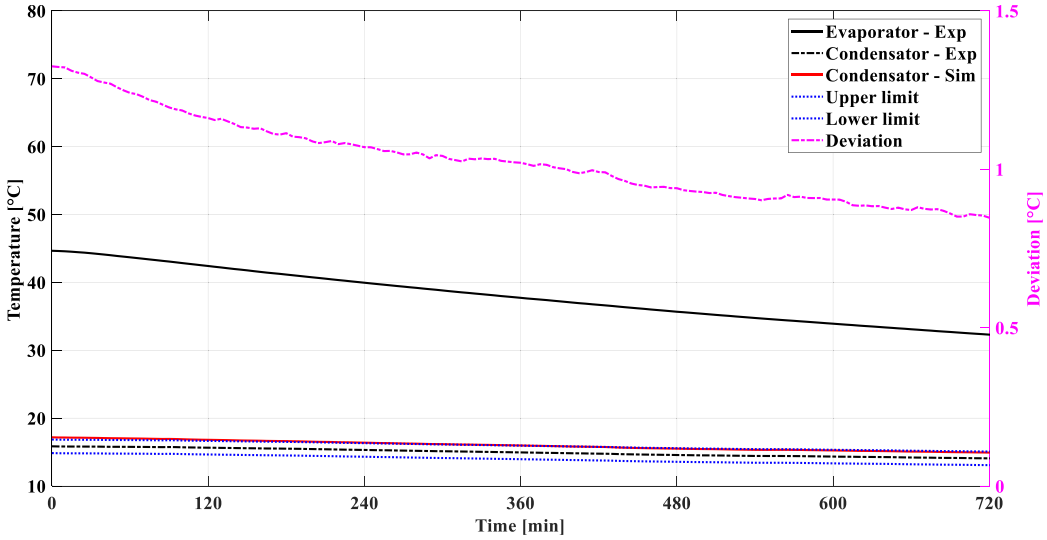

Fig. 10. Test 3 (reverse), experimental vs. Simulated temperature time histories. (For interpretation of the references to colour in this figure legend, the reader is referred to the web version of this article.)

$$MAPE = \frac{\left|y_{sim} - y_{exp}\right| / y_{exp}}{N_{measures}} \times 100 \tag{10}$$

$$R^2 = \frac{\sum_{i=1}^{N_{measures}} \left(y_{sim,i} - mean(y_{sim})\right)^2 - \sum_{i=1}^{N_{measures}} \left(y_{sim,i} - a_{reg,line} - b_{reg,line} \cdot y_{exp,i}\right)^2}{\sum_{i=1}^{N_{measures}} \left(y_{sim,i} - mean(y_{sim})\right)^2} \tag{11}$$

By evaluating these indexes for the investigated experimental tests, it is possible to obtain the results presented in Table 2.

From the reported values, it is possible to notice that excellent agreements are achieved. However, it worth noticing that higher differences occur in case of reverse mode simulation. From the presented results, it is possible to state that the PLVTD model is validated and reliable to be adopted for further analyses.

3. HyPVT concept description

The previously described PLVTD prototype is the core element of the novel solar photovoltaic thermal collector concept. Specifically, the conceived hybrid collector is an Integrated Collector Storage Solar Water Heater (ICSSWH), based on the previously described Planar Liquid Vapour Thermal Diode (PLVTD) and called the HyPVT. At the time of writing, the complete device has not been realized yet and thus the focus of this present work is to theoretically analyse the device performance to validate and support its fabrication. The proposed device structure is presented in Fig. 12 where the five different components can be detected: (i) transparent cover; (ii) photovoltaic absorber; (iii) PLVTD; (iv) integrated hot water storage tank, and (v) thermal insulation.

Concerning the device dimensions, it is 1.4 m high and 0.7 m wide with a total frontal area of 0.98 m^2. Other key dimensions are presented in Table 3.

Finally, the PV sheet is a monocrystalline silicon panel, with a nominal efficiency of around 17% and its behaviour is presented within

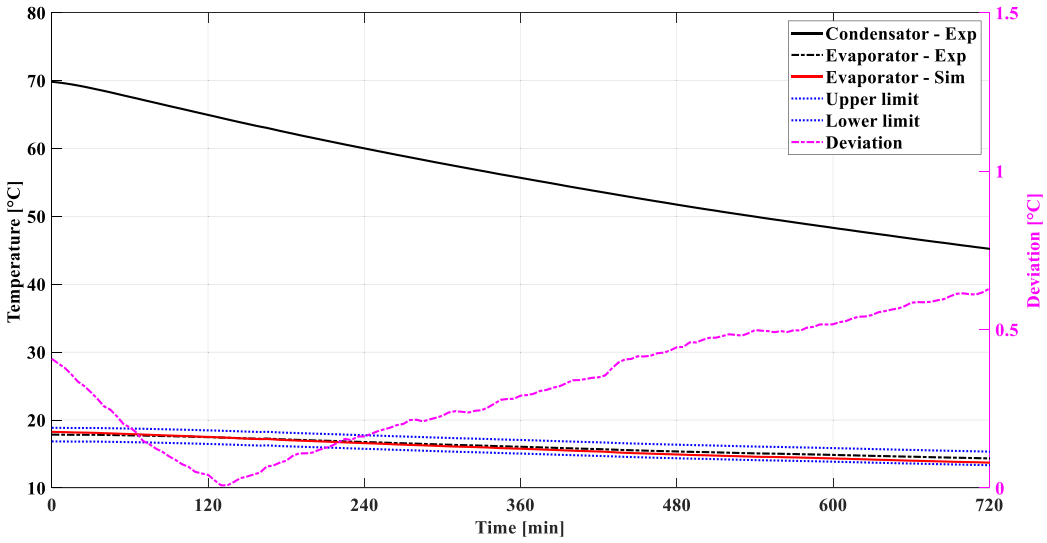

Fig. 11. Test 4 (reverse), experimental vs. Simulated temperature time histories. (For interpretation of the references to colour in this figure legend, the reader is referred to the web version of this article.)

Table 2
Validation indexes for all the investigated tests.

	Forward		*Reverse*	
	Test 1	*Test 2*	*Test 3*	*Test 4*
MAPE	0.13	0.11	0.51	0.28
R^2	0.99	0.99	0.93	0.97

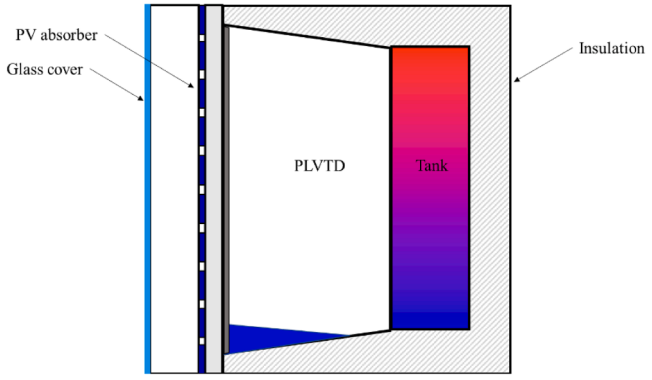

Fig. 12. Proposed prototype schematic representation.

the mathematical model. By integrating the PLVTD, the described device varies the front thermal resistance (R_{front}) from the heat collection to the heat retention phases. Specifically, thanks to the high heat transfer coefficient (low R_{front}) of the PLVTD during the forward phase, the entire device allows heat transfer during solar collection periods. On the other hand, during the reverse phase (when the PLVTD heat transfer coefficient drops, and the front thermal resistance rises), the conceived device can successfully retain the heat in the integrated thermal storage during non-collection periods (the heat retention phase). Concerning the HyPVT behaviour during the heat collection phase, the incident solar radiation is absorbed by the PV panel (a de facto collecting absorber) and partially converted into electricity. Incident solar radiation that is converted into heat is transferred through the PLVTD (characterized by a low thermal resistance during this phase) into the integrated thermal store as hot water at the rear of the device. Conversely, during the heat retention phase, the stored heat inside the water tank is subject to reduced heat loss due to the heavily insulated walls and the PLVTD. Specifically, since no evaporation/condensation phenomena occurs, the PLVTD guarantees a low heat loss coefficient, reducing the heat dissipation. It is worth mentioning that even if the described HyPVT device has not been realized, a similar prototype has been experimentally investigated by the same authors, as reported in Smyth et al. (2019), Pugsley et al. (2019), Pugsley (2017). This device has the same dimensional and geometrical features relative the proposed HyPVT and adopts the same working principles. Nonetheless, a main difference between the novel HyPVT and the device presented in Smyth et al. (2019), Pugsley et al. (2019), Pugsley (2017) exists, in that the latter utilizes a water pump to keep the evaporator surface wet, whereas the presented HyPVT relies on the capillary wicking feature. Specifically, the wicking (sorption) material represents a more cost-effective benefit, since the passive operation reduces operating costs (no parasitic pump input), thereby increasing the reliability of the device with less components.

Table 3
HyPVT dimensional/geometrical feature.

Quantity	Value	Unity
Glass cover thickness	2	mm
Air gap thickness	33	mm
PV sheet	5	mm
PLVTD depth	100	mm
Water storage tank depth	100	mm
Polystyrene foam insulation	75	mm
Water storage tank volume	0.1	m^3

3.1. HyPVT mathematical model

In this section, the mathematical model of the HyPVT concept is described. The thermal network detailing the heat transfer phenomena occurring inside the device is shown in Fig. 13.

here, GA($\tau\alpha$) and E_{el} are the solar radiation absorbed and the electrical power produced by the PV panel, respectively. With respect to the temperatures, T_{amb} is the ambient air temperature, $T_{g,e}$ and $T_{g,i}$ are the transparent cover external and internal temperatures, respectively, $T_{pv,e}$ and $T_{pv,i}$ are the external and internal temperatures of the PV panel, respectively, $T_{cond,e}$ is the temperature of the condenser external surface, T_w is the water node temperature and $T_{i,e}$ is the external surface temperature of the insulated case. Regarding thermal resistances (Fig. 13), R_{sky}, is the radiative resistance between the glass cover and the sky, $R_{c,o}$

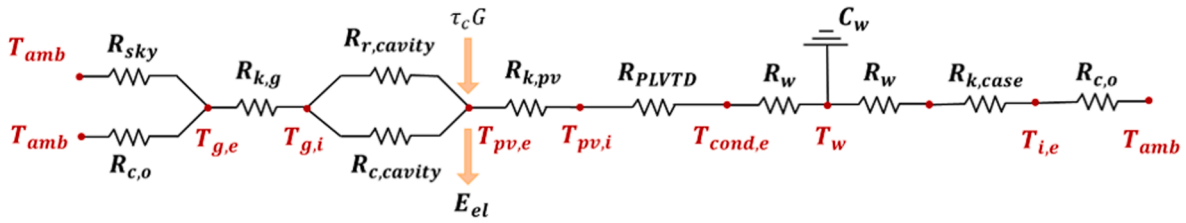

Fig. 13. HyPVT thermal network during the forward mode.

is the convective resistance between the glass cover and ambient air, $R_{k,g}$ is the conductive resistance inside the glass cover, $R_{r,cavity}$ is the radiative resistance of the air gap between the absorber and the glass, $R_{c,cavity}$ is the convective resistance between the absorber and the glass, $R_{k,pv}$ is the conductive resistance inside the PV panel, R_{PLVTD} is the thermal resistance of the PLVTD (assessed as previously shown), R_w is the thermal resistance of the water storage tank, and $R_{k,case}$ is the resistance of the HyPVT casing (including the insulating material). All the resistances presented in Fig. 13, with the exception of the PLVTD, are well-known convective, conductive and radiative heat transfer phenomena, and for sake of brevity, they are not specified here. Conversely, the term R_{PLVTD} describes the equivalent resistance of the PLVTD, which can be still evaluated as previously shown in this paper (see Eqs. (8) and (9)). With respect to the electricity produced by the PV panel (E_{el}), this has been evaluated, along with the electrical efficiency (η_{el}), by the following equations:

$$E_{el} = GA(\tau\alpha)\eta_{el} \tag{12}$$

$$\eta_{el} = \eta_{rif} \cdot \left(1 - \beta_{rif}\left(T_{pv,e} - T_{rif}\right)\right) \tag{13}$$

Where η_{el} is the overall electrical efficiency, η_{rif} is the PV nominal efficiency at reference test conditions, β_{rif} and T_{rif} are the temperature coefficient and the reference temperature of the PV panel (as per the data sheet) and T_{pv} is the PV panel temperature. The latter, is estimated through an energy balance of the PV panel control volume, as follows:

$$A_{diode}G(\tau\alpha) = E_{el} + \frac{\left(T_{pv,e} - T_{g,i}\right)}{R_{r,cavity}} + \frac{\left(T_{pv,e} - T_{g,i}\right)}{R_{c,cavity}} + \frac{\left(T_{pv,e} - T_{pv,i}\right)}{R_k} \tag{14}$$

With respect to the HyPVT thermal performance assessment, this is evaluated by adopting two different measures: (i) the front thermal resistance (R_{front}); and (ii) the heat collection and retention efficiencies. Concerning the former, the front thermal resistance is evaluated as follows (see Fig. 13):

$$R_{front} = R_W + R_{PLVTD} + R_{k,pv} + \left(R_{r,cavity}^{-1} + R_{c,cavity}^{-1}\right)^{-1} + R_{k,g} + \left(R_{sky}^{-1} + R_{c,o}^{-1}\right)^{-1} \tag{15}$$

here, the term R_{PLVTD} modifies its value according to the considered phase as specified before: during the heat collection phase, due the occurrence of evaporation/condensation phenomena, the PLVTD front thermal resistance is very low. On the contrary, during the reverse phase, since the evaporation/condensation phenomenon cannot take place, the front thermal resistance is high, reducing the heat losses. With respect to the heat collection and retention efficiencies it is instead necessary to estimate the heat stored and then lost during the device operations. More precisely, given any time interval $(\theta - (\theta - 1))$, where θ is the time, it is possible to evaluate the thermal energy variation (ΔQ_{tank}) inside the water storage as follows:

$$\Delta Q_{tank} = \sum_{\theta}^{\theta+1} M_w \cdot c_{p,v} \cdot \left[T_w(\theta) - T_w(\theta - 1)\right] \tag{16}$$

Where, M_w is the water mass inside the storage tank, T_w is the temperature of the water and c_p is the specific heat capacity of the water. By evaluating Eq. (16) from the starting interval ($\theta = 0$), to the end of the collection period ($\theta = \theta_{end,coll}$) it is possible to calculate the amount of energy stored inside the tank ($\Delta Q_{tank,coll}$), whereas, by evaluating Eq. (16) from the end of the collection period ($\theta = \theta_{end,coll}$) to the end of the retention period ($\theta = \theta_{end,ret}$), it is possible to calculate the energy lost from the device during the reverse operating condition ($\Delta Q_{tank,ret}$). Given these values, for the forward mode it is possible to define a collection efficiency as the ratio between the energy collected by the water tank at the end of the collection period ($\theta_{end,coll}$) and the total solar energy incident on the absorber during the same period ($Q_{sol,incident}$), as described in the following equation:

$$\eta_{collection} = \left(\frac{\Delta Q_{tank,coll}}{\Delta Q_{sol,incident}}\right) \cdot 100 \tag{17}$$

With respect to the reverse mode, the retention efficiency can be evaluated by considering the initial and final water tank temperatures, as follows:

$$\eta_{reverse} = 1 - \frac{T_w\left(\theta_{end,coll}\right) - T_w\left(\theta_{end,ret}\right)}{T_w\left(\theta_{end,coll}\right) - T_{amb}\left(\theta_{end,ret}\right)} \tag{18}$$

Where, T_w ($\theta_{end,coll}$) is the water temperature inside the store at the end of the collection period and T_w ($\theta_{end,ret}$) and T_{amb} ($\theta_{end,ret}$) are the water temperature inside the store and the ambient air temperature at the end of the retention period, respectively. By means of Eqs. (17) and (18) it is possible to evaluate the investigated ICSSWH heat collection and retention performances.

4. HyPVT theoretical performances

The described dynamic simulation tool has been adopted to determine the HyPVT theoretical performance and to verify its convenience over similar device without PLVTD. In this context, two different analyses have been performed: (i) first, the developed tool is used to evaluate the HyPVT performance at the variation of the boundary conditions to derive its collection efficiency curves, and (ii) secondly it is used to perform a comparison with a similar device, without the PLVTD (a standard ICSSWH collector) aiming to prove the potential of the HyPVT concept.

HyPVT theoretical performance assessment

The first analysis considered four different constant irradiation levels (see Table 4) with a constant air temperature of 25 °C (standard air temperature for testing conditions). The four simulations were carried out for an entire forward/reverse cycle consisting of six hours collection mode and ten hours of retention.

For each tests the related collection and retention efficiencies have been calculated using Eqs. (17) and (18) respectively over a six- and a

Table 4
Investigated boundary conditions.

	Test 1	Test 2	Test 3	Test 4
Irradiation [W/m^2]	1000	800	600	400
T_{amb} [°C]	25			

ten-hours period, and the results are shown in Table 5.

From the results it is possible to notice that, besides the interesting collection efficiency also remarkable 10 h retention ones are achieved. It worth noticing that these results are influenced by the different thermal resistance of the HYPVT front side during the forward and reverse mode. Specifically, the front side thermal resistance has been calculated by using Eq. (15) and its values for the collection and retention phases are equal to 0.2 m^2 K/W for the collection phase, and equal to 1.4 m^2 K/W for the reverse one. Aiming at better characterizing the collection efficiency of the device, the same Eqs. (17) and (18) have been applied over smaller time intervals (rather than on a daily basis) four the simulated tests reported in Table 4. The obtained collection efficiencies have been plotted against the normalized tank temperature (Pugsley, 2017) as shown in Fig. 14.

HyPVT performance comparison

To verify the convenience of the conceived HyPVT device, a comparison with a similar one based on the same dimensions and thermophysical features (e.g. solar absorption area, storage tank volume, materials, etc.), but without PLVTD, has been conducted. Specifically, the configurations reported in Fig. 15, and described in the following, have been investigated:

- *Device 1*: the proposed ICSSWH with a fully integrated PLVTD. In this case, the evaporation and condensation phenomena can occur during the forward mode, whereas only radiation and conduction phenomena take place during the reverse one.
- *Device 2*: the ICSSWH collector without a PLVTD. In this case, the solar radiation collected is directly transmitted to the water in the storage tank, as in a standard device. Nonetheless, higher losses are expected. This device has the same storage volume and active capture area as the other device.

The described devices are compared considering three different measures: (i) front thermal resistances during both forward and reverse phases; (ii) water tank temperature time histories; and (iii) collection and retention efficiencies. With respect to the front thermal resistances, evaluated as shown in Eq. (15), these are reported in Table 6. From the table it is possible to notice that, during the collection (forward) phase, the standard device (no PLVTD) is characterized by lower thermal resistance with respect to the proposed HyPVT.

Such a result is due to the fact that the PLVTD, even if highly transmissive during the forward mode due to the evaporation/condensation phenomenon, still contributes to the overall thermal resistances (absorber and condenser plates, wick layer, pillars, etc.). On the other hand, in case of the standard device (device 2 in Fig. 15), the absorber (PV sheet) is directly in contact with the storage tank, implying a lower front thermal resistance (and thus a higher heat transfer coefficient). Still, during the collection phase, the heat transfer coefficients of the proposed HyPVT and of the standard device as still comparable in terms of magnitude (0.22 vs. 0.20 m^2 K/W). Conversely, a different situation occurs during the retention phase, where the proposed HyPVT device exhibits a front thermal resistance remarkably higher than the standard ICSSWH (1.4 vs. 0.20 m^2 K/W). From the results shown in Table 6 it is then possible to state that the PLVTD integration does not really affects the heat collection performance of the device, while substantially enhance the heat retention ones. To verify the better performance expected by the HyPVT over the standard device, they are both investigated by means of the developed dynamic simulation tool by considering the same boundary conditions reported in Table 4, and the related results are shown in Fig. 16. Here, the water tank temperature time profiles are presented over a forward/reverse cycle made up of six hours in collection mode and ten in retention mode for both investigated configurations.

Table 5
Collection and retention efficiencies for the investigated working conditions.

	Test 1	Test 2	Test 3	Test 4
Reached collection temperature (6 h) [°C]	51.3	45.7	40.0	34.5
Collection efficiency [%]	52.0	51.1	49.8	47.2
Reached retention temperature (10 h) [°C]	47.3	42.5	37.5	32.7
Retention efficiency [%]	85.1	84.5	83.2	80.3

From the figure it is possible to notice that the HyPVT (device 1 in Fig. 15) and the standard ICSSWH (device 2 in Fig. 15) during the forward mode exhibit a similar profile, with device 2 performing slightly better than device 1, as expected in accordance to the results reported in Table 6. This slight difference is due to the higher thermal resistances between the PV panel/absorber and the water tank in device 1 opposed to the direct contact between the PV panel and storage tank in device 2 (as already specified). However, during the retention phase, the proposed HyPVT (device 1) experiences a smaller temperature drop compared to a standard ICSSWH without a thermal diode (device 2), in accordance with the front thermal resistance values reported in Table 6 for the reverse mode. As an example, for the case with a radiation of 1000 W/m^2, after 10 h of reverse mode the water temperature of device 1 (solid blue line in Fig. 16) is still around 47 °C, whereas device 2 (dotted blue line in Fig. 16) is 44 °C. The collection and retention efficiencies of the investigated tests are presented in Table 7. From the table, as expected, the collection efficiencies for both devices are comparable, whilst the retention efficiencies are different, and specifically always higher in case of the proposed HyPVT.

The results shown in Table 7 and Fig. 16 clearly indicate the validity of the proposed HyPVT collector concept giving positive theoretical results, that demonstrate a higher overall performance compared to a standard ICSSWH device based on similar dimensions and geometrical features and thus proving the case for PLVTD integration.

5. Conclusions

In this manuscript a novel Hybrid Photovoltaic Thermal (HyPVT) Integrated Collector Storage Solar Water Heater (ICSSWH) concept is presented and theoretically investigated. The innovative device integrates a novel Planar Liquid Vapour Thermal Diode (PLVTD) developed and experimentally tested at Ulster University, Belfast, Northern Ireland. Aimed at assessing the PLVTD performance under diverse boundary and operating conditions, a mathematical model was developed, and experimentally validated. The validated PLVTD mathematical model was incorporated into a more complex simulation tool conceived to analyse the physical behaviour of the proposed ICSSWH-HyPVT-PLVTD collector concept. The resulting tool is then adopted to verify the convenience of the inclusion of the PLVTD into ICSSWH collectors by performing comparison simulations. Specifically, the proposed HyPVT device performance were compared to that from a standard ICSSWH collector, with similar dimensions and thermophysical features, but with no PLVTD. The results demonstrated that the PLVTD plays an essential role in increasing the ICSSWH's overall thermal efficiency. In particular, the following conclusions can be drawn:

- The adoption of PLVTD into ICSSWH permits to have different collector's front thermal resistance during the heat collection and heat retention phases. More precisely, the HyPVT shows front thermal resistance of 0.22 m^2 K/W during the collection phase and of 1.4 m^2 K/W during the retention phase.
- The higher front thermal resistance during the retention phase permits to increase the retention efficiency with respect to a similar device not integrating the PLVTD;
- Whilst a slight reduction on the forward mode, the proposed HyPVT device had a 14% better heat retention efficiency in the reverse mode over the standard device.

By concluding, thermal diodes offer a promising solution to enhancing ICSSWH performance, enabling them to overcome some of

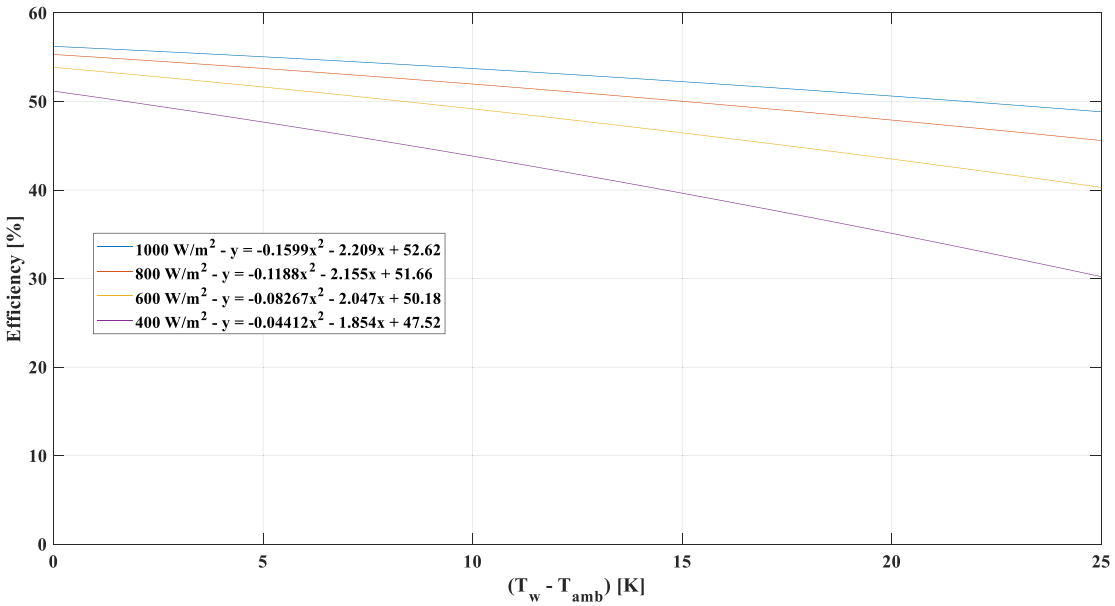

Fig. 14. Collection efficiency curves for the investigated HyPVT.

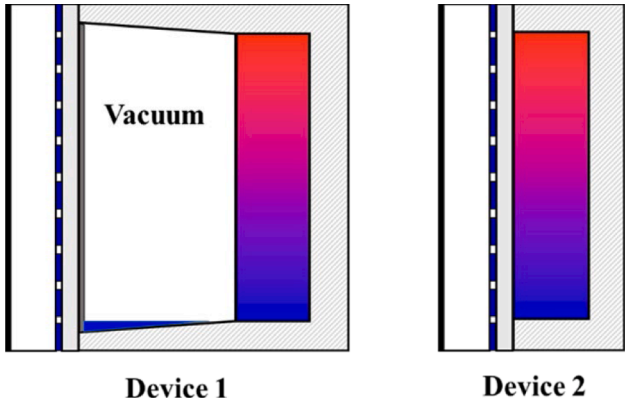

Fig. 15. Investigated device configurations.

Table 6
Front thermal resistances for the investigated devices.

		Device 1 (HyPVT)	Device 2 (standard)
Front thermal resistance (collection phase)	[m^2 K/W]	0.22	0.20
Front thermal resistance (retention phase)		1.4	

their main drawbacks and supporting their adoption in colder climatic regions previously beyond the reach of standard systems.

6. Future research

This research presented a dynamic simulation tool for the performance assessment of an ICSSWH-HyPVT collector integrating a novel PLVTD. The mathematical tool was adopted to confirm the benefits of the collector concept over devices with similar geometry. As next step, the developed mathematical model will be employed to support the development and physical fabrication of the HyPVT prototype. It is proposed that the tool will optimize the selection of componentry, inform sizing, and direct operational features to realize an actual protype that advances the thermal diode performance. Following suitable testing, overall validation of the simulation tool will be confirmed, and its application used to evaluate the concept performance in diverse climates and operating conditions over extended operating periods.

Nomenclature

Symbols

A	Surface area
BISS	Building Integrated Solar System
c	Specific Heat
G	Incident solar radiation
HyPVT	Hybrid Photovoltaic Thermal Collector
HTF	Heat Transfer Fluid
ICS	Integrated Collector Storage
ICSSWH	Integrated Collector Storage Solar Water Heater
K	Thermal conductivity
M	Mass
P	Pressure
PLVTD	Planar Liquid Vapour Thermal Diode
Q	Heat
Q_L	Latent heat
R	Thermal Resistance
R_{vap}	Universal Gas Constant
s	Thickness
T	Temperature
TD	Thermal Diode
V	Volume Flow Rate

Subscript

amb	Ambient air
coll	Collection
con	Condensator
cond	Condensation
e	External
el	Electric
eq	Equivalent
ev	Evaporator
evap	Evaporation

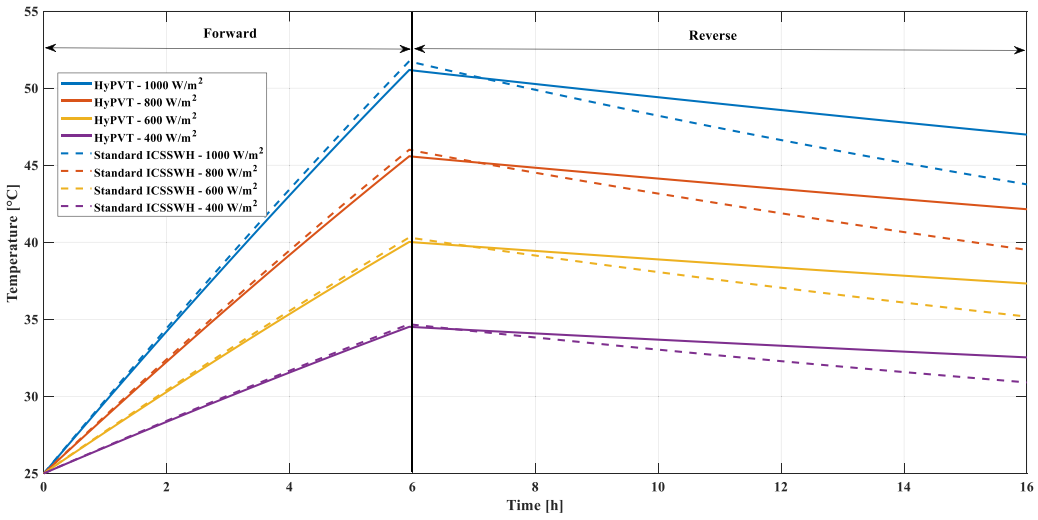

Fig. 16. HyPVT vs. standard ICSSWH water tank temperature/time profiles for the investigated tests.

Table 7
Collection and retention efficiencies for the investigated devices.

		Device 1 (HyPVT)	Device 2 (standard)
Test 1 (1000 W/m^2 & 25 °C)	Collection efficiency [%]	52.0	53.1
	Retention efficiency [%]	85.1	70.0
Test 2 (800 W/m^2 & 25 °C)	Collection efficiency [%]	51.1	51.9
	Retention efficiency [%]	84.5	69.0
Test 3 (600 W/m^2 & 25 °C)	Collection efficiency [%]	49.8	50.5
	Retention efficiency [%]	83.2	66.4
Test 4 (400 W/m^2 & 25 °C)	Collection efficiency [%]	47.2	47.9
	Retention efficiency [%]	80.3	60.9

g Glass
i Internal
k Conductive
o Outside
pv Photovoltaic
rad Radiative
ret Retention
rif Referment
sol Solar
Sky Sky vault
w Water

Greek

α Absorption coefficient
η Efficiency
ε Emissivity
θ Time
σ Stefan–Boltzmann constant
τ Transmission coefficient

CRediT authorship contribution statement

Annamaria Buonomanoa: Conceptualization, Methodology, Model development, Formal analysis, Investigation, Data curation, Writing – original draft, Writing – review & editing, Visualization, Supervision. **Cesare forzano:** Conceptualization, Methodology, Model development, Formal analysis, Investigation, Data curation, Writing – original draft, Writing – review & editing, Visualization, Supervision. **Adrian Pugsley:** Conceptualization, Methodology, Model development, Formal analysis, Investigation, Data curation, Writing – original draft, Writing – review & editing, Visualization, Supervision. **Mervyn Smyth:** Conceptualization, Methodology, Model development, Formal analysis, Investigation, Data curation, Writing – original draft, Writing – review & editing, Visualization, Supervision.

Declaration of competing interest

The authors declare that they have no known competing financial interests or personal relationships that could have appeared to influence the work reported in this paper.

Data availability

Data will be made available on request.

References

Agency, I.E., 2003. Key World Energy Statistics. IEA Washington, DC.
Anupam Rao, Y., Somwanshi, A., 2022. A comprehensive review on integrated collector-storage solar water heaters. Mater. Today Proc. 63, 15–26.
Bakhtavar, E., et al., 2020. Assessment of renewable energy-based strategies for net-zero energy communities: A planning model using multi-objective goal programming. J. Clean. Prod. 272, 122886.
Baljit, S.S.S., Chan, H.-Y., Sopian, K., 2016. Review of building integrated applications of photovoltaic and solar thermal systems. J. Clean. Prod. 137, 677–689.
Barone, G., Buonomano, A., Forzano, C., Giuzio, G.F., Palombo, A., 2021. Supporting the sustainable energy transition in the canary islands: simulation and optimization of multiple energy system layouts and economic scenarios. Front. Sustain. Cities 3.
Barone, G., et al., 2019. Solar thermal collectors. In: Solar Hydrogen Production: Processes, Systems and Technologies, pp. 151–178.
Barone, G., et al., 2020. Enhancing trains envelope – heating, ventilation, and air conditioning systems: A new dynamic simulation approach for energy, economic, environmental impact and thermal comfort analyses. Energy 204.
Barone, G., et al., 2021a. Implementing the dynamic simulation approach for the design and optimization of ships energy systems: Methodology and applicability to modern cruise ships. Renew. Sustain. Energy Rev. 150.
Barone, G., et al., 2021b. Increasing renewable energy penetration and energy independence of island communities: A novel dynamic simulation approach for energy, economic, and environmental analysis, and optimization. J. Clean. Prod. 311.
Barone, G., et al., 2022. A prototypal high-vacuum integrated collector storage solar water heater: Experimentation, design, and optimization through a new in-house 3D dynamic simulation model. Energy 238, 122065.

Buonomano, A., Barone, G., Forzano, C., 2002. Advanced energy technologies, methods, and policies to support the sustainable development of energy, water and environment systems. Energy Rep. 8, 4844–4853.
Buonomano, A., Forzano, C., Palombo, A., Russo, G., 2023a. Solar-assisted district heating networks: development and experimental validation of a novel simulation tool for the energy optimization. Energy Convers. Manage. 288, 117133.
Buonomano, A., Papa, G. Del, Giuzio, G. Francesco, Polombo, A., Russo, G., 2023b. Future pathways for decarbonization and energy efficiency of ports: modelling and optimization as sustainable energy hubs. J. Cleaner Prod. 420, 138389.
Ceglia, F., et al., 2022. An energy, environmental, management and economic analysis of energy efficient system towards renewable energy community: The case study of multi-purpose energy community. J. Clean. Prod. 369, 133269.
Chandrasekar, M., Senthilkumar, T., 2021. Five decades of evolution of solar photovoltaic thermal (PVT) technology – A critical insight on review articles. J. Clean. Prod. 322, 128997.
Forzano, C., et al., 2019. Building integrating phase change materials: A dynamic hygrothermal simulation model for system analysis. J. Sustain. Dev. Energy Water Environ. Syst. 7 (2), 325–342.
Gagliano, A., et al., 2021. Analysis of the performances of a building-integrated PV/Thermal system. J. Clean. Prod. 320, 128876.
Ghosh, A., 2020. Potential of building integrated and attached/applied photovoltaic (BIPV/BAPV) for adaptive less energy-hungry building's skin: A comprehensive review. J. Clean. Prod. 276, 123343.
Graziani, F.M., 2017. Directive of the European parliament and of the council on the promotion of the use of energy from renewable sources (recast).
International Energy Agency, I.E.A., 2014. Sustainable Energy for All 2013-2014: Global Tracking Framework Report. The World Bank.
Lamnatou, C., et al., 2018. Building-integrated solar thermal system with/without phase change material: Life cycle assessment based on ReCiPe, USEtox and ecological footprint. J. Clean. Prod. 193, 672–683.
Martínez Fernández, P., et al., 2019. A review of modelling and optimisation methods applied to railways energy consumption. J. Clean. Prod. 222, 153–162.
Maturo, A., et al., 2021. Design and environmental sustainability assessment of energy-independent communities: The case study of a livestock farm in the North of Italy. Energy Rep. 7, 8091–8107.
Messaouda, A., et al., 2020. Analysis of an integrated collector storage system with vacuum glazing and compound parabolic concentrator. Appl. Therm. Eng. 169, 114958.
Mohamad, A.A., 1997. Integrated solar collector–storage tank system with thermal diode. Sol. Energy 61 (3), 211–218.
Muhumuza, R., et al., 2019a. Experimental investigation of horizontally operating thermal diode solar water heaters with differing absorber materials under simulated conditions. Renew. Energy 138, 1051–1064.
Muhumuza, R., et al., 2019b. Experimental study of heat retention performance of thermal diode integrated collector storage solar water heater (ICSSWH) configurations. Sustain. Energy Technol. Assess. 34, 214–219.
Panahi, R., et al., 2019. Analysis of the thermal efficiency of a compound parabolic integrated collector storage solar water heater in Kerman, Iran. Sustain. Energy Technol. Assess. 36, 100564.
Pugsley, A., 2017. Theoretical and experimental analysis of a novel flat photovoltaic-thermal solar water heater with integrated energy storage via a planar liquid-vapour thermal diode.
Pugsley, A., et al., 2019. Theoretical and experimental analysis of a horizontal planar liquid-vapour thermal diode (PLVTD). Int. J. Heat Mass Transfer 144, 118660.
Sharma, A., Chauhan, R., 2022. Integrated and separate collector storage type low-temperature solar water heating systems with latent heat storage: A review. Sustain. Energy Technol. Assess. 51, 101935.
Singh, R., Lazarus, I.J., Souliotis, M., 2016. Recent developments in integrated collector storage (ICS) solar water heaters: A review. Renew. Sustain. Energy Rev. 54, 270–298.
Smyth, M., et al., 2017. The evolutionary thermal performance and development of a novel thermal diode pre-heat solar water heater under simulated heat flux conditions. Renew. Energy 113, 1160–1167.
Smyth, M., et al., 2018. The experimental evaluation and improvements of a novel thermal diode pre-heat solar water heater under simulated solar conditions. Renew. Energy 121, 116–122.
Smyth, M., et al., 2019. Experimental performance characterisation of a hybrid photovoltaic/Solar Thermal Façade module compared to a flat integrated collector storage solar water heater module. Renew. Energy 137, 137–143.
Smyth, M., et al., 2020a. Experimental characterisation of different hermetically sealed horizontal, cylindrical double vessel integrated collector storage solar water heating (ICSSWH) prototypes. Sol. Energy 206, 695–707.
Smyth, M., et al., 2020b. Modelling and experimental evaluation of an innovative integrated collector storage solar water heating (ICSSWH) prototype. Renew. Energy 157, 974–986.
Sopian, K., et al., 2004. Performance of a non-metallic unglazed solar water heater with integrated storage system. Renew. Energy 29 (9), 1421–1430.
Souliotis, M., et al., 2011. Heat retaining integrated collector storage solar water heater with asymmetric CPC reflector. Sol. Energy 85 (10), 2474–2487.
Souliotis, M., et al., 2017. Integrated collector storage solar water heater under partial vacuum. Energy 139, 991–1002.
Tripanagnostopoulos, Y., Souliotis, M., 2006. ICS solar systems with two water tanks. Renew. Energy 29 (1), 13–38.
Vassiliades, C., et al., 2022. Building integration of active solar energy systems: A review of geometrical and architectural characteristics. Renew. Sustain. Energy Rev. 164.
Xie, Y., et al., 2022. Numerical investigation of the effect factors on the performance of a novel PV integrated collector storage solar water heater. Renew. Energy 195, 1354–1367.
Yassen, T.A., Mokhlif, N.D., Eleiwi, M.A., 2019. Performance investigation of an integrated solar water heater with corrugated absorber surface for domestic use. Renew. Energy 138, 852–860.
Zhang, H., et al., 2019. Energy consumption optimization of train operation for railway systems: Algorithm development and real-world case study. J. Clean. Prod. 214, 1024–1037.